Available online at www.sciencedirect.com

ScienceDirect

Transportation Research Procedia 00 (2018) 000–000

Transportation Research Procedia

www.elsevier.com/locate/procedia

World Conference on Transport Research - WCTR 2019 Mumbai 26-31 May 2019

A simulation study on the optimal pattern of speed reduction markings affecting speed choice before curve entry

Hirofumi Yotsutsuji[a]*, Toshimori Otazawa[b], Hideyuki Kita[b]

[a] *CERI, PWRI, 1-3-1-34 Hiragishi, Toyohira-ku, Sapporo, Hokkaido 062-8602, Japan*
[b] *Kobe University, 1-1 Rokkodai, Nada-ku, Kobe, Hyogo 657-8501, Japan*

Abstract

Speed reduction markings (SRMs) on road surface are transverse marking lines with decreasing spacing in the direction of vehicle movement, which are installed in order to encourage drivers to reduce their vehicle speed safely. The driver of a leading vehicle moving on SRM-installed lane toward a curve may be exposed to accident risk due to shortage of deceleration and rear-end collision between the leading and following vehicles. To avoid such risk, the decreasing spacing pattern of the marking lines needs to be optimized according to the trajectory of speed of the leading vehicle. The aim of this study is to examine the optimal pattern of SRMs by simulating the optimal speed trajectory of the leading vehicle and the risk of rear-end collision of the following vehicle. To achieve this aim, we construct an optimal control model of driving behavior with speed perception and combine it with a car-following model. In the case of SRMs before the sharp bend, our numerical examples have shown the results as follows: 1) There is the case that the spacing pattern in which decreasing rate is greater in the end section than in the remaining sections may produce a high risk of the rear-end collision before the curve entry, although the leading vehicle safely enters the curve. 2) There is the case that the spacing pattern in which the decreasing rate is zero in all sections may produce an accident with which the leading driver meets within the curve, although the collision risk is very few. These results indicate that the optimal pattern of SRMs must consider not only the optimal speed trajectory of the leading vehicle but also the risk of rear-end collision before the curve entry.

Peer-review under responsibility of WORLD CONFERENCE ON TRANSPORT RESEARCH SOCIETY.

Keywords: Speed reduction markings ; Spacing pattern ; Driver perception ; Dynamic optimization ; MCMC estimation ; Rear-end collision risk

1. Introduction

Speed reduction markings (SRMs) on road surface are transverse marking lines with decreasing spacing in the direction of vehicle movement. When SRMs are installed on a straight lane adjacent to a transition curve section, it is

* Corresponding author. Tel.: +81-11-841-1738; fax: +81-11-841-9747.
E-mail address: yotsutsuji-h@ceri.go.jp

Peer-review under responsibility of WORLD CONFERENCE ON TRANSPORT RESEARCH SOCIETY

expected that SRMs encourage drivers to reduce their vehicle speed safely before they enter the curve. The Manual on Uniform Traffic Control Devices, MUTCD (FHWA, 2009) explains that the effect of speed reduction of SRMs is caused by a pattern of progressively reduced spacing to give the drivers the impression that their speed is increasing. However, MUTCD does not explain the optimal spacing pattern commensurate with the curve radius. The driver of a leading vehicle moving on SRM-installed lane toward the curve may be exposed to accident risk due to shortage of deceleration and rear-end collision between the leading and following vehicles. MUTCD has not given sufficient conditions for prevention of such risk to SRMs yet. In order to avoid such risk, the spacing pattern of SRMs needs to be optimized according to vehicular speed trajectories of the leading vehicle approaching the curve.

The aim of this study is to examine the optimal spacing pattern of SRMs affecting the leading driver's speed choice before the curve entry by simulating the optimal speed trajectory of the leading vehicle, and examine the risk of rear-end collision of the following vehicle. To achieve this aim, we construct an optimal control model of driving behavior with speed perception, which is based on Pontryagin's maximum principle, and combine it with a car-following model to estimate PICUD in terms of the rear-end collision risk.

The body of this paper consists of seven chapters. Chapter 2 describes two mathematical models. One is a model regarding perception and behavior of the leading driver, and the other is a model of car-following behavior to show a risk index called PICUD. Chapter 3 describes how to solve the optimal control problem regarding the perception and behavior of the leading driver and how to estimate the model parameters. Chapter 4 describes details of simulation data obtained from a driving simulation experiment that has already been conducted in our previous study. Chapters 5, 6 and 7 describe simulation results, discussion and conclusion, respectively.

2. Modeling

2.1. Perception and behavior of leading driver

We impose assumptions on modeling speed perception and driving behavior of the leading driver, as follows:

Firstly, as for the speed perception of the leading driver travelling on SRM-installed lane toward the curve, we set the following assumptions. This driver can recognize a maximum safe speed, $\hat{v}_{\mathrm{O}}$, of the curve as $\hat{v}_{\mathrm{S}}$ on the way to the curve. In this study, subjective and objective values of the vehicle speed are denoted by the indices "S" and "O", respectively. The maximum safe speed means the maximum value of the vehicle speed at which the driver can safely pass through the curve. In short, $\hat{v}_{\mathrm{O}}$ and $\hat{v}_{\mathrm{S}}$ are defined by geometry of the curve and speed perception of the driver, respectively. The important points are that these speeds are independent with respect to t and SRMs cannot affect these speeds at all. In addition, the driver can perceive a vehicle speed, $v_{\mathrm{O}}(t)$, as $v_{\mathrm{S}}(t)$ while operating the vehicle at time t. When the driver perceives $v_{\mathrm{O}}(t)$ as $v_{\mathrm{S}}(t)$, there is a case that a discrepancy occurs between $v_{\mathrm{S}}(t)$ and $v_{\mathrm{O}}(t)$. Then, $v_{\mathrm{S}}(t)$ can only be affected by the spacing pattern of SRMs through visual speed perception of the driver. The derivative of the vehicle speed with respect to time, $\dot{v}_{\mathrm{O}}(t)$, is proportional to the derivative of the perceived speed with respect to time, $\dot{v}_{\mathrm{S}}(t)$. When $v_{\mathrm{O}}(t)$ exceeds $\hat{v}_{\mathrm{O}}$ (or $\hat{v}_{S}$), speeding accidents occur within the curve.

Secondly, as for the driving behavior of the leading driver, we set the following assumptions. The driver chooses a speed to maximize a utility which is defined by $v_{\mathrm{S}}(t)$ under condition of $\hat{v}_{\mathrm{S}}$. In this study, this utility, which is expressed as $U(v_{\mathrm{S}}(t)|\hat{v}_{\mathrm{S}})$, is referred to as "speed utility". The driver at the beginning location of SRM-installed lane can draw out a plan to enter the curve safely, by use of dynamic optimization technique. Then, the driver can maximize the sum of present discounted value of $U(v_{\mathrm{S}}(t)|\hat{v}_{\mathrm{S}})$ that the driver will obtain at every step on SRM-installed lane, in order to enter the curve at the optimal vehicle speed. The driver operates the vehicle in accordance with the plan that the driver has already drawn out at the beginning location of SRM-installed lane.

Now, the optimal control problem that the driver should solve at the beginning location of SRM-installed lane can be formulated as follows (Chiang, 1992):

$$\underset{v_{\mathrm{S}}(0),\cdots,v_{\mathrm{S}}(T)}{\text{Maximize}} \int_0^T U(v_{\mathrm{S}}(t)|\hat{v}_{\mathrm{S}}) \exp[-\sigma t]\,\mathrm{d}t, \tag{1}$$

$$\text{subject to} \quad f(v_{\mathrm{O}}(t), L(t)) = v_{\mathrm{S}}(t) + \dot{v}_{\mathrm{S}}(t), \tag{2}$$

$$\dot{v}_{\mathrm{S}}(t) = \alpha \dot{v}_{\mathrm{O}}(t), \tag{3}$$

$$f(v_{\mathrm{O}}(t), L(t)) = \left\{1 + L(t)^{-\xi}\right\} v_{\mathrm{O}}(t), \tag{4}$$

$$v_{\mathrm{O}}(0) = \bar{v}_{\mathrm{O}} > 0, \tag{5}$$

$$v_{\mathrm{O}}(T) \exp[-\bar{\sigma} T] \geq 0, \tag{6}$$

$$U(v_{\mathrm{S}}(t) | \hat{v}_{\mathrm{S}}) = \mu v_{\mathrm{S}}(t) - \exp[\mu\{v_{\mathrm{S}}(t) - \hat{v}_{\mathrm{S}}\}], \tag{7}$$

where,
$v_{\mathrm{S}}(t)$: instantaneous speed perceived by the leading driver at time t,
$v_{\mathrm{O}}(t)$: instantaneous speed of the leading vehicle at time t,
$\hat{v}_{\mathrm{S}}$: maximum safe speed recognized by the leading driver,
$L(t)$: line interval of SRMs at time t,
$\dot{v}_{\mathrm{S}}(t)$: derivative of $v_{\mathrm{S}}(t)$ with respect to t,
$\dot{v}_{\mathrm{O}}(t)$: derivative of $v_{\mathrm{O}}(t)$ with respect to t,
σ : discount rate of time preference,
α, ξ : parameters,
μ : degree of risk aversion,
t : continuous time from at the beginning of SRMs at time $t = 0$ to at the end of that at time $t = T$.

Equation (1) expresses how to maximize the sum of present discounted value of $U(v_{\mathrm{S}}(t)|\hat{v}_{\mathrm{S}})$ that is obtained at every steps on SRM-installed lane. Equation (7) formulates $U(v_{\mathrm{S}}(t)|\hat{v}_{\mathrm{S}})$ in the concrete. The first term of equation (7) means that the speed utility increases when $v_{\mathrm{S}}(t)$ increases, so that this term is the comfort of driving. The second term means that the speed utility decreases when the difference between $v_{\mathrm{S}}(t)$ and $\hat{v}_{\mathrm{S}}$ increases, so that this term is the safety of driving. When σ increases, the driver is more likely to underestimate the speed utility at the curve entry. When μ increases, the driver is more likely to feel the risk of accidents in the situation of high speed.

Equation (2) expresses how the driver perceives $v_{\mathrm{S}}(t)$ through the visual perception as to $v_{\mathrm{O}}(t)$ and $L(t)$, where $L(t)$ is a control variable. In this study, function f is referred to as "optic flow function". Equation (2) represents that the difference between the optic flow produced by $v_{\mathrm{O}}(t)$ and $L(t)$ and the perceived speed, $v_{\mathrm{S}}(t)$, is equivalent to the derivative of $v_{\mathrm{S}}(t)$ with respect to t. In short, $f(v_{\mathrm{O}}(t), L(t)) - v_{\mathrm{S}}(t)$ is equivalent to $\dot{v}_{\mathrm{S}}(t)$.

The optic flow is visual information that the driver can obtain while driving (Lee, 1976). Equation (4) gives the optic flow function, f, a concrete shape. The driver is watching SRMs flowing at relative speed against the vehicle speed. The driver perceives the vehicle speed because of this optic flow. The spacing pattern of SRMs affects the perception of the optic flow. Parameter ξ is the effect of the spacing pattern on the visual perception.

Equation (3) expresses that $\dot{v}_{\mathrm{S}}(t)$ is proportional to $\dot{v}_{\mathrm{O}}(t)$ and the proportionality coefficient, α, is independent from time. Thus, equation (3) assumes that there is a systematic discrepancy between $\dot{v}_{\mathrm{S}}(t)$ and $\dot{v}_{\mathrm{O}}(t)$.

Finally, equations (5) and (6) express initial condition and transversality condition, respectively (Chiang, 1992).

2.2. Risk of rear-end collision of following vehicle

In this study, we apply a car-following model to evaluate the risk of rear-end collision of the following vehicle. Especially, we select the Kometani-Sasaki model (Kometani & Sasaki, 1958) that can describe the car-following behavior when acceleration and deceleration of the leading vehicle affect the behavior of the following vehicle. The model can be described as follows:

$$\dot{v}_{\mathrm{O}}^{\mathrm{F}}(t + T) = \beta_1 \left\{v_{\mathrm{O}}^{\mathrm{L}}(t) - v_{\mathrm{O}}^{\mathrm{F}}(t)\right\} + \beta_2 \dot{v}_{\mathrm{O}}^{\mathrm{L}}(t), \tag{8}$$

where,

$v_{\mathrm{O}}^{\mathrm{F}}(t)$: instantaneous speed of the following vehicle at time t,
$v_{\mathrm{O}}^{\mathrm{L}}(t)$: instantaneous speed of the leading vehicle at time t,
T : time of delayed reaction,
β_1, β_2: parameters.

The first term of equation (8) means a factor of the following driver's reaction against the difference of speeds between the leading and following vehicles. The second term means a factor of the leading driver's reaction against the acceleration and deceleration of the leading vehicle (Kometani & Sasaki, 1958).

In this study, we use a major index regarding the rear-end collision, which is a possibility index for collision with urgent deceleration (PICUD) (Uno, et al., 2002). This index relates to the collision distance. When PICUD is less than zero, the following vehicle is no longer able to avoid the rear-end collision in the situation of urgent deceleration of the leading vehicle. PICUD can be described as follows:

$$r_{\mathrm{PICUD}} = \frac{v_{\mathrm{O}}^{\mathrm{L}}(t)^2}{-2\phi} + \bar{s}(t) - \left\{ v_{\mathrm{O}}^{\mathrm{F}}(t)\Delta t + \frac{v_{\mathrm{O}}^{\mathrm{F}}(t)^2}{-2\phi} \right\}, \tag{9}$$

where,
ϕ : degree of deceleration in the situation of the urgent collision,
$\bar{s}(t)$: distance headway in the situation of the urgent deceleration at time t,
Δt : time between the urgent deceleration of the leading vehicle and the braking of the following vehicle.

3. Solution

3.1. Solving the optimal control problem

The Lagrangian, Φ, of the optimal control problem expressed by equations (1) to (7) can be formulated by using the Hamiltonian, H, as follows (see Appendix A):

$$\Phi = \int_0^T H[v_{\mathrm{S}}(t), v_{\mathrm{O}}(t), L(t), \lambda(t)]\mathrm{d}t + \int_0^T \dot{\lambda}(t) v_{\mathrm{S}}(t)\mathrm{d}t - \lambda(T) v_{\mathrm{S}}(T) + \lambda(0) v_{\mathrm{S}}(0) + \eta v_{\mathrm{O}}(T) \exp[-\bar{\sigma} T], \tag{10}$$

$$H[v_{\mathrm{S}}(t), v_{\mathrm{O}}(t), L(t), \lambda(t)] = U(v_{\mathrm{S}}(t) | \hat{v}_{\mathrm{S}}) \exp[-\sigma t] + \lambda(t)\left\{ f\left(v_{\mathrm{O}}(t), L(t)\right) - v_{\mathrm{S}}(t) \right\}. \tag{11}$$

The first-order condition to maximize the Lagrangian, Φ, can derive the following function (see Appendix A).

$$\dot{v}_{\mathrm{S}}(t) = \left\{ \frac{1 + L(t)^{-\xi}}{\alpha} - \sigma \right\} \frac{1 - \exp[\mu\{v_{\mathrm{S}}(t) - \hat{v}_{\mathrm{S}}\}]}{\mu \exp[\mu\{v_{\mathrm{S}}(t) - \hat{v}_{\mathrm{S}}\}]}. \tag{12}$$

Equation (13) describes that $\dot{v}_{\mathrm{S}}(t)$ can be determined by $L(t)$, $v_{\mathrm{S}}(t)$, $\hat{v}_{\mathrm{S}}$, ξ, α, σ and μ.

3.2. Estimating the model parameters

Equations (2), (3) and (4) can derive the following equation.

$$v_{\mathrm{S}}(t) = \left\{ 1 + L(t)^{-\xi} \right\} v_{\mathrm{O}}(t) - \alpha \dot{v}_{\mathrm{O}}(t). \tag{13}$$

By substituting equation (14) into equation (13), the following equation can be derived.

$$1 + L(t)^{-\xi} - \alpha \cdot \left\{ \sigma + \frac{\mu \alpha v_{\mathrm{O}}(t) \exp\left[\mu\left\{\left\{1 + L(t)^{-\xi}\right\} v_{\mathrm{O}}(t) - \alpha \dot{v}_{\mathrm{O}}(t) - \hat{v}_{\mathrm{S}}\right\}\right]}{1 - \exp\left[\mu\left\{\left\{1 + L(t)^{-\xi}\right\} v_{\mathrm{O}}(t) - \alpha \dot{v}_{\mathrm{O}}(t) - \hat{v}_{\mathrm{S}}\right\}\right]} \right\} = 0. \tag{14}$$

Now, we define the error function, Ψ, that is normally distributed with mean 0 and variance ρ, as follows:

$$\Psi[\alpha,\xi|v_{\mathrm{O}}(t),L(t);\hat{v}_{\mathrm{S}},\mu,\sigma]=1+L(t)^{-\xi}-\alpha\cdot\left\{\sigma+\frac{\mu\alpha v_{\mathrm{O}}(t)\exp\left[\mu\left\{\{1+L(t)^{-\xi}\}v_{\mathrm{O}}(t)-\alpha\dot{v}_{\mathrm{O}}(t)-\hat{v}_{\mathrm{S}}\right\}\right]}{1-\exp\left[\mu\left\{\{1+L(t)^{-\xi}\}v_{\mathrm{O}}(t)-\alpha\dot{v}_{\mathrm{O}}(t)-\hat{v}_{\mathrm{S}}\right\}\right]}\right\}. \tag{15}$$

Accordingly, the likelihood function, $\mathcal{L}$, can be defined as follows:

$$\mathcal{L}(\alpha,\xi|v_{\mathrm{O}}(t),L(t);\hat{v}_{\mathrm{S}},\mu,\sigma,\rho)=\prod_{t=0}^{T}\frac{1}{\sqrt{2\pi}\rho}exp\left[-\frac{\Psi[\alpha,\xi|v_{\mathrm{O}}(t),L(t);\hat{v}_{\mathrm{S}},\mu,\sigma]^2}{2\rho^2}\right]. \tag{16}$$

The log-likelihood function of equation (17) becomes a multiple peak function that is overlapping many convex upward functions. Thus, when we estimate the parameters to maximize this log-likelihood function, the Newton-Raphson method does not specify unique solution because of convergence at a local solution. Therefore, we use the Markov chain Monte Carlo (MCMC) method based on the Metropolis-Hastings algorithm (Chib & Greenberg, 1995) in order to estimate the parameters to converge at a global solution.

4. Simulation data

4.1. Inputs

We must prepare input data in order to simulate both the optimal speed trajectory of the leading vehicle and the rear-end collision risk. In addition, because of the difficulty of simulation, we must set several parameters as constant parameters. In the model of the leading driver, the discount rate of time preference, σ, the degree of risk aversion, μ, and the speed of the leading vehicle at the initial time, $\bar{v}_{\mathrm{O}}\equiv v_{\mathrm{O}}^{\mathrm{L}}(0)$ are given as constant parameters. In the model of the following driver, the time of delayed reaction, T, and the coefficients, β_1,β_2, are given as constant parameters. For the parameters of the rear-end collision risk, the degree of deceleration, ϕ, and the time between the urgent deceleration of the leading vehicle and the braking of the following vehicle, Δt, are given as constant parameters. Under the assumption that σ and μ are given, we estimate parameters α and ξ by using the input data with respect to $v_{\mathrm{O}}(t)$, $\dot{v}_{\mathrm{O}}(t)$ and $L(t)$. In this study, we use data obtained from a driving simulation experiment that we have already been conducted in our previous study (Yotsutsuji, 2017).

4.2. The experiment

To define a few key terms in this study, let us shortly explain the contents of the driving simulation experiment in our previous study.

In the experiment, we employed a fixed-base driving simulator using software named UC-win/Road Driving Sim, which can display at a rate of 120 frames per second. The total width of the roadway was 13 m, comprising two 3.5 m lanes, a 1.5 m median strip, two 1.75 m left shoulders, and two 0.5 m right shoulders. The width of each transverse marking line of SRMs was 45 cm. The curve radius was varied between 200 m and 1,000 m in increments of 100 m. In this study, we focus on the curve radius of 200 m, as a sharp bend.

A lane equipped with SRMs was longitudinally divided into several ranges, which is referred to as “section”. The spacing pattern was dealt with as the spatial arrangement of the transverse marking lines in every section, in which the spacing was equal within an arbitrary section and decreasing between two adjacent sections toward the curve. The “decrease ratio (DR)” of line spacing between two adjacent sections was defined as an index that was calculated by dividing the difference between the “spacing length in the forward section” and the “spacing length in the backward section” by the “spacing length in the backward section”. Thus, in this study, the problem of adjusting the spacing pattern according to a change in the curve radius is replaced by that of finding the optimal location of the greatest DR section in accordance with changes in the curve radius.

In the experiment, 20 people were openly recruited as participants, including 10 elderly people aged 65 years or older. During the experiment, although the speedometer was displayed on screen in 100 m of the first section in SRM-installed lane, it was not displayed in the remaining sections. An experimenter instructed each of participants to

Table 1. Configuration of spacing pattern of SRMs (Yotsutsuji, 2017)

Pattern	Greater DR section	Section name Length [m]	Z 100	I 100	II 100	III 100	IV 100	V 100
A	Constant	Spacing [m]	12.00	12.00	12.00	12.00	12.00	12.00
		DR [%]	0	0	0	0	0	0
B	Beginning	Spacing [m]	12.00	10.29	9.18	8.72	8.28	7.87
		DR [%]	0	15	10	5	5	5
C	Middle	Spacing [m]	12.00	11.40	10.26	8.72	7.85	7.46
		DR [%]	0	5	10	15	10	5
D	End	Spacing [m]	12.00	11.40	10.83	10.29	9.26	7.87
		DR [%]	0	5	5	5	10	15

accelerate to 80 km/h by 100 m of the first section, and to keep their driving speed at 80 km/h as constant as possible in the remaining sections without watching the speedometer, and to pass the curve safely by decelerating as necessary.

Table 1 shows the four spacing patterns labelled A, B, C and D, which we focus on in this study. Pattern A has a DR of zero in all sections and is used as a baseline. Pattern B, C and D have higher DRs in the beginning, middle and end sections, respectively, compared with the other sections. The driver run in sections Z to V toward the curve.

5. Simulation results

5.1. Numerical example of the leading driver's behavior

Figure 1 shows a numerical example regarding the behavior of the leading driver with $\sigma = 0.5$ and $\mu = 0.3$ in the case of the curve radius of 200 m, corresponding to the four spacing patterns.

In Figure 1, horizontal axis represents the distance to the transition curve section, in which the origin denotes the beginning location of section Z, and the right hand of the axis is toward the curve. Longitudinal axis represents the vehicle speed, $v_{\mathrm{O}}(t)$, the speed perceived by the driver, $v_{\mathrm{S}}(t)$, and the maximum safe speed recognized by the driver, $\hat{v}_{\mathrm{S}}$. The values that are just located on the longitudinal axis corresponding to the origin represent the initial speeds, which means $v_{\mathrm{O}}(0)$ and $v_{\mathrm{S}}(0)$.

In Figure 1, the initial values of $v_{\mathrm{O}}(t)$ are equivalent among the four spacing patterns, and $v_{\mathrm{O}}(0)$ is numerically equal to $v_{\mathrm{S}}(0)$ in all of the spacing patterns. In addition, $v_{\mathrm{O}}(0)$, $v_{\mathrm{S}}(0)$, $\hat{v}_{\mathrm{S}}$ are set as 27.8 m/s (100 km/h), 27.8 m/s (100 km/h), and 16.7 m/s (60 m/h), respectively. With regard to curve radii corresponding to road design speed of 60 km/h, a desired minimum radius of the curve is 200 m (JRA, 2004). In Figure 1, the maximum safe speed recognized by the driver, $\hat{v}_{\mathrm{S}}$, is assumed to be equal to the road design speed, $\hat{v}_{\mathrm{O}}$, corresponding to the desired minimum curve radius.

Figure 1 describes the following results: In the case of pattern A, both values of $v_{\mathrm{O}}(t)$ and $v_{\mathrm{S}}(t)$ have exceeded $\hat{v}_{\mathrm{O}}$ (that is $\hat{v}_{\mathrm{S}}$) in the end of section V. In the cases of pattern B and C, although the value of $v_{\mathrm{S}}(t)$ has dipped below $\hat{v}_{\mathrm{O}}$ before the end of section V, the value of $v_{\mathrm{O}}(t)$ has exceeded $\hat{v}_{\mathrm{O}}$ in the end of section V. In the case of pattern D, both values of $v_{\mathrm{O}}(t)$ and $v_{\mathrm{S}}(t)$ have dipped below $\hat{v}_{\mathrm{O}}$ before the end of section V.

5.2. Numerical example of the rear-end collision risk

Figure 2 shows a numerical examples regarding the rear-end collision risk that the following vehicle collides with the leading vehicle operated by the driver with $\sigma = 0.5$ and $\mu = 0.3$ in the case of the curve radius of 200 m.

In Figure 2, horizontal axis represents the travel time to the transition curve section, in which the origin denotes the beginning location of section Z, and the right hand of the axis is toward the curve. Longitudinal axis represents the values of PICUD.

As for ϕ and Δt, we set them as ϕ = -3.0 [m/s^2] and $\Delta t = 1.25$ [s]. As for β_1, β_2, T, and $\mathrm{v}_{\mathrm{O}}^{\mathrm{F}}(0)$, we set them as $\beta_1 = 0.3$, $\beta_2 = 0.3$, $T = 1.25$ s, and $\mathrm{v}_{\mathrm{O}}^{\mathrm{F}}(0) = 28.0$ m/s.

Figure 2 describes the results that PICUD under pattern A, B, C and D are 14.1 m, 3.0 m, 7.1 m and 0.3 m in the end of section V, respectively. Accordingly, in terms of PICUD, there is the case that pattern D may produce a high risk of the rear-end collision before the curve entry.

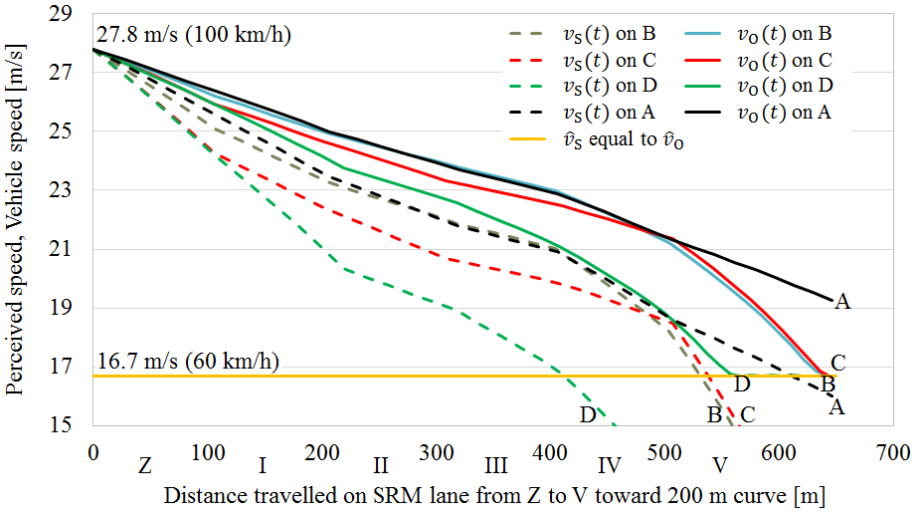

Figure 1. Trajectory of perceived speed and vehicle speed simulated by the optimal control model

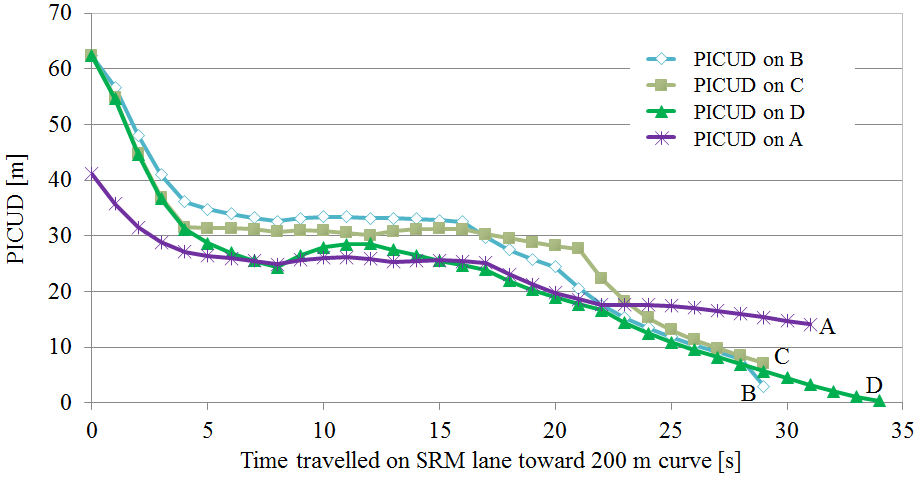

Figure 2. Trajectory of rear-end collision risk measured by PICUD

6. Discussion

The numerical examples shown in Figures 1 and 2 correspond to the case that there is a sharp bend continuous with SRM-installed lane on which the leading driver begins to travel with high speed at the initial time and has the risk of rear-end collision of the following vehicle before entering the curve. In this case, our numerical examples have shown the results as follows:

- There is the case that the spacing pattern of SRMs in which the decreasing rate is greater in the end section than in the remaining sections may produce a high risk of the rear-end collision before the curve entry, although the leading vehicle safely enters the curve.
- There is the case that the spacing pattern in which the decreasing rate is zero in all sections may produce an accident with which the leading driver meets within the curve, although the collision risk is very few.

In each of the four spacing patterns, as the leading driver is approaching the curve, discrepancy between the perceived speed and the vehicle speed increases progressively with the decreasing distance from the curve. At the same time, movements of the discrepancy are different among the spacing patterns. We consider that one of the reasons why this phenomenon gives rise to is that, when the leading driver decelerates on SRM-installed lane in order to drop the perceived speed down below the maximum safe speed at the timing of the curve entry, the spacing pattern of SRMs can hasten or delay the timing of such drop-down situation. We can see this because Figure 1 shows that the drop-down points are the point near 400 m for pattern D, the point near 550 m for patterns B and C, and the point over 600 m for pattern A. Even though the timing of the drop-down situation with respect to the perceived speed can be hastened, the vehicle speed is not always dropped down below the maximum safe speed before the curve entry. We can see this because Figure 1 shows that the discrepancy of speeds in patterns B and C remains at the point of 600 m, although the perceived speed has already been dropped down at the point near 550 m.

7. Conclusion

In this study, we numerically simulated both the optimal speed trajectory of the leading vehicle moving on SRM-installed lane toward the curve and the risk of rear-end collision of the following vehicle, and examined the optimal spacing pattern of SRMs affecting the leading driver's speed choice before the curve entry. We constructed the optimal control model that described the driving behavior with speed perception in accordance, and estimated the collision risk by using PICUD. Our simulation results indicated that the optimal pattern of SRMs had to consider not only the optimal speed trajectory of the leading vehicle but also the risk of rear-end collision of the following vehicle before the curve entry.

There remains some topics that should be explored in the future works. Regarding the speed utility function, $U(v_{\mathrm{S}}(t)|\hat{v}_{\mathrm{S}})$, we assumed that, without any explanation, each of the perceived speed, $v_{\mathrm{S}}(t)$, and the degree of risk aversion, μ, independently affected the utility. The relationship between perception and risk aversion must explain to be clear. Regarding the rear-end collision risk, we dealt with only two vehicles. Analyzing the effect of SRMs on adjustment of platoon speed will be required. Furthermore, regarding the empirical study, we will have to verify that the spacing pattern of SRMs needs to vary according to the curve radius, by use of causal inference.

Acknowledgements

This study was carried out during first-author's previous employment at Kobe University, by using data from a driving simulation experiment financially supported by a collaborative research project between Kobe University and NEXCO RI. This study received financial support from JSPS Grant-in-Aid for Scientific Research (B) No. 16H03017. The authors express our gratitude for constructive suggestions from Dr. Jian Xing and Prof. Takamasa Iyo, and thank to Mr. Kazuki Kitamura who did several calculations as part of his graduation work at Kobe University.

Appendix A. Solution of the optimal control problem expressed by equations (1) to (7)

The Lagrangian, Φ, is defined as follows:

$$\Phi = \int_0^T U(v_{\mathrm{S}}(t)|\hat{v}_{\mathrm{S}}) \exp[-\sigma t]\,\mathrm{d}t + \int_0^T \lambda(t)\{f(v_{\mathrm{O}}(t), L(t)) - v_{\mathrm{S}}(t) - \alpha \dot{v}_{\mathrm{O}}(t)\}\mathrm{d}t + \eta v_{\mathrm{O}}(T) \exp[-\bar{\sigma} T]. \quad \text{(A1)}$$

To derive the Hamiltonian, we prepare the derivative of $\lambda(t)v_{\mathrm{S}}(t)$ and $\alpha\lambda(t)v_{\mathrm{O}}(t)$, as follows:

$$\frac{\mathrm{d}}{\mathrm{d}t}[\lambda(t)v_{\mathrm{S}}(t)] = \dot{\lambda}(t)v_{\mathrm{S}}(t) + \lambda(t)\dot{v}_{\mathrm{S}}(t) = \dot{\lambda}(t)v_{\mathrm{S}}(t) + \alpha\lambda(t)\dot{v}_{\mathrm{O}}(t), \quad \text{(A2)}$$

$$\frac{\mathrm{d}}{\mathrm{d}t}[\alpha\lambda(t)v_{\mathrm{O}}(t)] = \alpha\dot{\lambda}(t)v_{\mathrm{O}}(t) + \alpha\lambda(t)\dot{v}_{\mathrm{O}}(t). \quad \text{(A3)}$$

By integrating both side of each of equations (A2) and (A3), we obtain the following equations.

$$\int_0^T \alpha\lambda(t)\dot{v}_{\mathrm{O}}(t)\mathrm{d}t = \int_0^T \frac{\mathrm{d}}{\mathrm{d}t}[\lambda(t)v_{\mathrm{S}}(t)]\mathrm{d}t - \int_0^T \dot{\lambda}(t)v_{\mathrm{S}}(t)\mathrm{d}t = \lambda(T)v_{\mathrm{S}}(T) - \lambda(0)v_{\mathrm{S}}(0) - \int_0^T \dot{\lambda}(t)v_{\mathrm{S}}(t)\mathrm{d}t, \quad \text{(A4)}$$

$$\int_0^T \alpha\lambda(t)\dot{v}_{\mathrm{O}}(t)\mathrm{d}t = \int_0^T \frac{\mathrm{d}}{\mathrm{d}t}[\alpha\lambda(t)v_{\mathrm{O}}(t)]\mathrm{d}t - \int_0^T \alpha\dot{\lambda}(t)v_{\mathrm{O}}(t)\mathrm{d}t. \quad \text{(A5)}$$

By substituting equation (A4) into equation (A1), we obtain equations (11) and (12). Now, the first-order conditions with respect to $v_{\mathrm{S}}(t)$, $v_{\mathrm{O}}(t)$ and $\lambda(t)$ are derived from Lagrangian Φ, as follows:

$$\frac{\mathrm{d}}{\mathrm{d}v_{\mathrm{S}}} U(v_{\mathrm{S}}(t)|\hat{v}_{\mathrm{S}}) \exp[-\sigma t] - \lambda(t) = U'(v_{\mathrm{S}}(t)|\hat{v}_{\mathrm{S}}) \exp[-\sigma t] - \lambda(t) = 0, \quad \text{(A6)}$$

$$\lambda(t) \frac{\mathrm{d}}{\mathrm{d}v_{\mathrm{O}}} f\big(v_{\mathrm{O}}(t), L(t)\big) + \alpha\dot{\lambda}(t) = 0, \quad \text{(A7)}$$

$$f(v_{\mathrm{O}}(t), L(t)) = v_{\mathrm{S}}(t) + \dot{v}_{\mathrm{S}}(t). \quad \text{(A8)}$$

By differentiating equation (A6) with respect to t, we obtain the following equation.

$$\dot{\lambda}(t) = -\sigma U'(v_{\mathrm{S}}(t)|\hat{v}_{\mathrm{S}}) \exp[-\sigma t] + U''(v_{\mathrm{S}}(t)|\hat{v}_{\mathrm{S}})\dot{v}_{\mathrm{S}}(t) \exp[-\sigma t]. \quad \text{(A9)}$$

By substituting equation (A9) into equation (A7), we obtain the following equation.

$$\frac{\mathrm{d}}{\mathrm{d}v_{\mathrm{O}}} f\big(v_{\mathrm{O}}(t), L(t)\big) = \alpha\left\{\sigma - \frac{U''\big(v_{\mathrm{S}}(t)\big|\hat{v}_{\mathrm{S}}\big)\dot{v}_{\mathrm{S}}(t)}{U'\big(v_{\mathrm{S}}(t)\big|\hat{v}_{\mathrm{S}}\big)}\right\}. \quad \text{(A10)}$$

Finally, by substituting the derivative of equation (4) with respect to $v_{\mathrm{O}}(t)$ into equation (A10), we obtain the following equation.

$$1 + L(t)^{-\xi} = \alpha\left\{\sigma - \frac{U''\big(v_{\mathrm{S}}(t)\big|\hat{v}_{\mathrm{S}}\big)\dot{v}_{\mathrm{S}}(t)}{U'\big(v_{\mathrm{S}}(t)\big|\hat{v}_{\mathrm{S}}\big)}\right\}. \quad \text{(A11)}$$

By substituting the derivative of equation (7) with respect to $v_{\mathrm{S}}(t)$ into equation (A11), we obtain equation (13).

References

Chiang, A. C. 1992. Elements of dynamic optimization. McGaw-Hill.

Chib, S., Greenberg, E. 1995. Understanding the Metropolis-Hastings algorithm. The American Statistician 49.4, 327-335.

Federal Highway Administration 2009. Speed reduction markings. Manual on Uniform Traffic Control Devices (MUTCD) 3B.22, 393-394.

Hayward, J. C. 1972. Near-miss determination through use of a scale of danger. Highway Research Record 384, 24-34.

Japan Road Association 2004. Explanation and Application of Road Structure Ordinance. Maruzen, 309-320.

Kometani, E., Sasaki, T. 1958. On the stability of traffic flow (Report-I). Journal of Operational Research 2.1, 11-16.

Lee, D. N. 1976. A theory of visual control of braking based on information about time-to-collision. Perception 5.4, 437-459.

Uno, N., Iida, Y., Itsubo, S., Yasuhara, S. 2002. A microscopic analysis of traffic conflict caused by lane-changing vehicle at weaving section. In Proceedings of the 13th Mini-EURO Conference-Handling Uncertainty in the Analysis of Traffic and Transportation Systems, Bari, Italy.

Yotsutsuji, H. (2017). Does array pattern of speed reduction markings need to be changed in accordance with horizontal curve radius?: causality analysis using driving simulator data. Journal of the Eastern Asia Society for Transportation Studies 12, 1904-1916.